Analytica Chimica Acta 1053 (2019) 139–147

Contents lists available at ScienceDirect

Analytica Chimica Acta

journal homepage: www.elsevier.com/locate/aca

Ultrasensitive detection of avian influenza A (H7N9) virus using surface-enhanced Raman scattering-based lateral flow immunoassay strips

Meng Xiao [a, 1], Kaixin Xie [a, 1], Xiaohui Dong [b, c, 1], Lei Wang [a], Caihong Huang [a], Fei Xu [a], Wei Xiao [a], Meilin Jin [b, c, *], Boyan Huang [a, **], Yong Tang [a, d, ***]

[a] Department of Bioengineering, Guangdong Province Engineering Research Center for Antibody Drug and Immunoassay, Jinan University, Guangzhou, 510632, PR China
[b] State Key Laboratory of Agricultural Microbiology, College of Veterinary Medicine, Huazhong Agricultural University, Wuhan, 430070, PR China
[c] Wuhan Keqian Biology Co., Ltd, Wuhan, 430000, PR China
[d] Institute of Food Safety and Nutrition, Jinan University, Guangzhou, 510632, PR China

HIGHLIGHTS

- An antibody-based Raman lateral flow immunoassay strip was developed for the AIV H7N9.
- AuAg^{4-ATP}@AgNPs was synthesized firstly to develop ultrabright SERS probes.
- SERE-LFIAS was three orders of magnitude more sensitive than the corresponding HA assays.

GRAPHICAL ABSTRACT

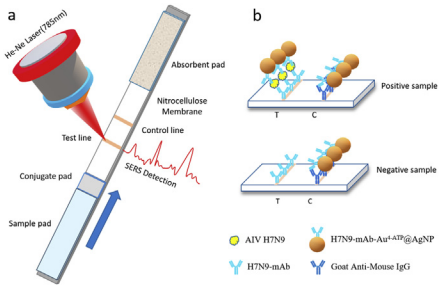

ARTICLE INFO

Article history:
Received 10 August 2018
Received in revised form
1 November 2018
Accepted 28 November 2018
Available online 7 December 2018

Keywords:
Avian influenza virus
AuAg^{4-ATP}@AgNPs
Surface-enhanced Raman scattering
Lateral flow immunoassay strips

ABSTRACT

The development of biosensors that are portable, low-cost, and quantitative has long been sought for rapid, on-site, and timely detection of avian influenza virus (AIV). In this study, an antibody-based Raman lateral flow immunoassay strip was developed to detect AIV H7N9. This LFIA strip used a novel core-shell structure material, AuAg^{4-ATP}@AgNPs, as a Raman probe. An antibody specific for AIV and goat anti-mouse IgG antibody were immobilized on a nitrocellulose membrane as the test and control lines, respectively. Accumulation of antibody-virus-antibody-Raman probe complex at the test line could be visualized by the naked eye, and the Raman signal could be quantified using a portable Raman instrument. The testing process for the SERS-based LFIA strips could be completed in 20 min, which avoided the time-cost of current methods for AIV analysis. In our SERS-based biosensor, we estimated the limit of detection (LOD) for H7N9 to be 0.0018 HAU. This value is approximately three orders of magnitude more sensitive than the corresponding HA assays. When testing real sample, the results of the strip test were in

* Corresponding author. Department of Bioengineering, Guangdong Province Engineering Research Center for Antibody Drug and Immunoassay, Jinan University, Guangzhou, 510632, PR China.
** Corresponding author.
*** Corresponding author. Department of Bioengineering, Guangdong Province Engineering Research Center for antibody drug and immunoassay, Jinan University, Guangzhou, 510632, PR China.
E-mail addresses: jinmeilin@mail.hzau.edu.cn (M. Jin), thboyan@jnu.edu.cn (B. Huang), tyjaq7926@163.com (Y. Tang).
[1] These authors contributed equally to the manuscript.

https://doi.org/10.1016/j.aca.2018.11.056

accordance with those from real-time PCR testing. In conclusion, the SERS-based LFIA strip proposed in this study shows tremendous potential to detect targets quickly and sensitively using an elegantly simple method.

1. Introduction

In point-of-care testing (POCT), lateral flow immunoassay (LFIA) strips are highly attractive biosensors [1–3]. They are widely used with diagnostic biomarkers as well as in infectious disease prevention and control, food safety, and environmental monitoring, due to their simplicity, low cost, and long-term stability [4–6]. In a typical test, sample is pulled through a stationary membrane by capillarity forces. The sample then passes through the test line and control line, where the nanoprobe is captured. An accumulation of nanoparticles results in the appearance of a visible signal on the capture line. Gold nanoparticles (GNPs) are commonly used as the nanoprobe in naked eye detection-based LFIA strips [7,8]. Colloidal gold chromatography has been used successfully for detection of various analytes and does not require complex sample preparation and an electrochemical or optical device to read test results [9,10]. However, because of their low sensitivity, colloidal gold strips are frequently associated with subjective judgment errors. Therefore, improving the sensitivity and quantification capabilities of LFIA strips could have a significant impact on the application of this technology.

To improve the performance of LFIA sensors, much effort has been devoted to signal amplification to meet the need for highly sensitivity detection. In the last decades, attempts to achieve sufficient sensitivity in LFIA sensors have included the integration of various nanomaterials, such as magnetic particles, carbon nanoparticles, fluorescent microspheres, quantum dots, up-conversion fluorescence, and Lanthanide nanoparticles [11–16]. When combined with a portable test strip reader for optical, magnetic, and electrochemical signal, the LFIA biosensor can accomplish rapid quantitative detection of the targets [17]. Because, in practice, the concentration of target analytes is usually very low, most of the existing methods described above are still troubled in some way by poor sensitivity and low accuracy [18]. For example, the color change on the detection line of conventional colloidal gold strips and the fluorescence intensity on the fluorescent strips usually do not provide sufficient signal strength and sensitivity. Surface-enhanced Raman scattering (SERS) is one ultrasensitive signal amplification method that allows for detection and analysis at very low concentrations [19]. Recently, SERS-based Lateral flow immunoassay (LFIA) sensors have been reported for highly sensitive and rapid detection of target biomarkers [20,21].

Synthesizing SERS tags with higher Raman signals is a key factor in improving the sensitivity and quantification capabilities of SERS-LFIAS sensors [22]. The use of immobilized metallic nanoparticles as Raman reporter molecules can generate strong SERS signals, and they are commonly applied as detection probes. Gold and silver nanoparticles are the most regularly used materials for preparing SERS tags. In general, the SERS effect of silver nanoparticles is 10–100 times that of gold nanoparticles, and the shape of the nanoparticles is also an influencing factor [23–25]. Recently, researchers have encapsulated Raman molecules between gold core and gold shell nanostructures to develop ultrabright SERS probes, which have shown great potential for many application, such as biomarker detection, tumor imaging, to name a few [26–29]. The Raman reporter trapped between the core and shell possesses an intense electromagnetic field (E field) enhancement, greatly heightening the Raman signal of the Raman reporter [30]. Moreover, the layer of the shell can effectively prevent the degradation of the SERS signal due to reporter desorption and also increase the stability of the SERS signal [28]. Herein, we report a novel core-shell SERS tag: $AuAg^{4-ATP}$@AgNPs, in which 4-aminothiophenol (4-ATP) is immobilized in the core-shell interstitial space as the Raman reporter. $AuAg^{4-ATP}$@AgNPs exhibited a strong SERS signal and displayed excellent stability in aqueous solution.

In the past decades, avian influenza virus has been a subject of widespread concern due to its ability to cause serious illnesses. These diseases are easily transmitted in poultry facilities, and this results in the possibility of transmission and infection in humans. Consequently, outbreaks and epidemics of AIV seriously threaten human health and the global economy [31,32]. According to differences in clinical pathogenicity, the disease group was divided into high pathogenic avian influenza virus (HPAIV) and low pathogenic avian influenza virus (LPAIV). The HPAIs hitherto found were mainly caused by the AIV H5, H7, and H9 subtype, which had high mortality rates. In 2013, there were cases of human HPAIV H7N9 reported in China. By the end of the year, 132 cases in total were reported, of which nearly 39 resulted in death [33]. The ability for prompt detection of these viruses is of the utmost importance in protecting both public health and the poultry economy. Virus isolation in embryonated chicken eggs (ECEs) is considered the gold standard for AIV detection, but complex procedures are time consuming [34]. Real-time polymerase chain reaction (RT-PCR) is a highly sensitive and fast method in virological monitoring, but high levels of amplification usually results in possible false positives [35]. Traditional immunochromatographic sensors are less sensitive and do not meet the needs of virus detection. Therefore, AIV monitoring and prevention requires the development of a sensitive, portable and rapid detection technology.

In recent years, researchers have combined SERS with immunochromatography systems to explore high-sensitivity detection of low-level biomarkers of viruses and bacteria [36,37]. In this study, we functionalized $AuAg^{4-ATP}$@AgNPs in combination with antibodies to develop an ultrasensitive SERS-LFIAS for detection of AIV H7N9. A silver shell layer covering the Raman reporter prevented the probes from aggregating at high concentration in the T line and C line. A color change in the test line effectively indicated the presence of target analytes for naked-eye detection, and the amount of virus expressed by the hemagglutination titer of AIV H7N9 [38]. Additionally, a quantitative result was obtained by measuring the SERS-tag signal intensity, which could provide early monitoring data in response to the emergence of a pandemic, allowing for timely deployment of effective preventive measures.

2. Experimental

2.1. Materials and apparatus

Chloroauric acid ($HAuCl_4 \cdot 3H_2O$), bovine serum albumin (BSA,98%), trisodium citrate (99.8%), polyethylene glycol (PEG, MW, 4000), polyvinylpyrrolidone (PVP, MW 29,000, powder), 4-aminothiophenol (4-ATP), and S-17 (Rhodasurf ON-870) were all

purchased from Sigma Chemicals Co., (St Louis, MO, USA). Tween-20, D-trehalose (99%), sucrose (99%), and L-ascorbic acid were obtained from AMRESCO Inc. (30175 Solon Industrial, Parkway, Solon, OH, USA). Silver nitrate ($AgNO_3$, crystal) was purchased from Tianjin Damao Chemical Reagent Factory (Tianjin, China). Goat anti-mouse immunoglobulin G (IgG) was obtained from Sungene Biotech Co., Ltd (Tianjin, China). AIV H7N9 monoclonal antibodies (mAb) and H7N9 samples were obtained from State Key Laboratory of Agricultural Microbiology (Huazhong Agricultural University, Wuhan). Inactivated AIV H7N9, H5N1 (Re-6, Re-7, Re-8), and subtype H9 were recombinant influenza viruses, produced by Harbin Weike Biotechnology Development Company (Harbin, China). The recombinant influenza viruses were cultured in chick-embryo culture. Then, the sample was inactivated and freeze-dried for further use. Nitrocellulose (NC) membranes, plastic backing, absorbent pads, conjugation pads, and sample pads were all purchased from JN Bio Co., Ltd (Shanghai, China). All other chemicals were of analytical grade and used without any further purification.

A transmission electron microscope (TEM, PHILIPS TECNAI, Holland), Scanning electron microscopy (SEM, Carl Zeiss AG, Germany), a Biodot XYZ3060 dispense platform (Biodot, Inc, USA), a Synergy H1 Hybrid Multi-Mode Microplate Reader (Bio Tek Instruments, Inc. USA), a Zetasizer Nano ZS (Malvern Panalytical Ltd.) and a centrifuge (Beckman, Germany) were used. A programmable strip cutter HGS201 was purchased from Shanghai Jiening Biotech (Shanghai, China). A portable Raman spectrometer was obtained from Guangzhou Biaoqi Electronic Technology Co., Ltd (Guangzhou, China). All aqueous solutions were prepared with double-distilled water (Millipore, Massachusetts, USA).

2.2. Preparation of mAb-AuAg^{4-ATP}@AgNPs

The preparation of the anti-H7N9 monoclonal antibody was detailed description in Supplementary Material. A positive hybridoma cells (6B3) was obtained to produce anti-H7N9 monoclonal antibodies (Table S1). The preparation of the mAb-AuAg^{4-ATP}@AgNPs probe is illustrated in Fig. 1. Colloidal gold particles were first prepared according to a previously reported method with slight modifications [39]. Generally, 100 mL of ultrapure water was heated to the point of boiling with vigorous stirring, and then 2 mL of 1% $HAuCl_4$ was added. After boiling again, 3 mL of 1% trisodium citrate was rapidly added. The mixture was boiled with agitation for 10 min and then cooled to 25 °C. To prepare AuAg^{4-ATP}@AgNPs, 64 μL of 100 mM vitamin C was added to 10 mL of colloidal gold solution and stirred for 5 min. Then, 160 μL of 10 mM $AgNO_3$ was added drop-wise to the mixture. After stirring for 20 min, a thin silver layer was covered in AuNPs, that is, as gold core and silver shell nanoparticles (Au@AgNPs). Next, 5 μL of a 1 mM 4-ATP solution was added and stirred for 30 min. Subsequently, 100 μL of 10% PVP was added as a protectant, Au@Ag^{4-ATP}NPs were purified by centrifugation, and then resuspended with the same volume of ultrapure water. Finally, vitamin C and silver nitrate were added twice in the above manner. The synthesis of AuAg^{4-ATP}@AgNPs were centrifuged at 6000 rcf/10 min and resuspended in 20 mL of ultrapure water.

The pH of the AuAg^{4-ATP}@AgNPs solution was adjusted to 8.5 using 0.25 M K_2CO_3, and then 1 mL of this solution was mixed with 10 μL of H7N9 mAb (1 mg/mL) and incubated for 1 h. Subsequently, 10 μL of 10% PVP was added to the mixture to block the surface of AuAg^{4-ATP}@AgNPs. After incubating for 1 h, the labeled mAb-AuAg^{4-ATP}@AgNPs probe was separated from the solution by centrifugation at 8000 RCF for 10 min, and then resuspended in 100 μL of buffer containing 0.1% PEG4000, 0.5% BSA, 0.5% Tween 20, 0.5% S-17, 20% sucrose, and 20% D-trehalose.

2.3. Preparation of SERS-LFIAS

The SERS-LFIAS consisted of a sample pad, absorbent pad, conjugation pad, NC membranes, and plastic backing. A desired volume of mAb-AuAg^{4-ATP}@AgNPs was dispensed onto the conjugation pad using a Biodot XYZ3060 dispense system. Then, H7N9 mAb (0.5 mg/mL) and goat anti-mouse IgG (1 mg/mL) were dispensed to the test line and control line on the NC membrane, respectively. Each antibody was dispensed at a rate of 1.0 μL/cm using dispense platform, followed by drying at 37 °C for 10 h. All the parts were assembled with a 2 mm overlap. The SERS-LFIAS was cut into individual 3.8-mm-wide strips using a programmable cutting machine. Each strip was fitted into a plastic housing for the further detection of Raman shift intensity using a portable Raman spectrometer.

2.4. Performance of SERS-LFIAS for H7N9 detection

Inactivated AIV H7N9 freeze-dried powder was dissolved in with 0.015 M PBS. Hemagglutination test indicated that hemagglutination titer of the inactivated AIV H7N9 sample is 512 HAU (Fig. S1). Then, the sample were diluted two-fold with 0.015 M PBS (e.g. 2.56, 1.28, 0.64, 0.32, 0.16, 0.08, 0.04, 0.02, 0.01, 0.005 and 0.0025 HAU).

75 μL sample containing a series of AIV H7N9 concentrations was added to the sample pad of SERS-LFIAS. The liquid migrated along the NC membrane toward the absorption pad through capillary action. After 20 min, the results of SERS-LFIAS were recorded using a mobile phone CCD camera and a portable Raman spectrometer (λ = 785 nm; power density, 60 mW/μm^2; acquisition time, 1 s). The SERS-LFIAS conditions were optimized and tested for sensitivity with the inactivated H7N9 virus as a positive sample. The specificity of the SERS-LFIAS was evaluated using AIV (H5N1 Re-6, H5N1 Re-7, H5N1 Re-8, H9) and other viruses (NDV La Sota, IBDV Gt) as test antigens. The various antigens were diluted with PBS to 0.32 HAU and added individually onto SERS-LFIAS, after which the results were read using a portable Raman spectrometer.

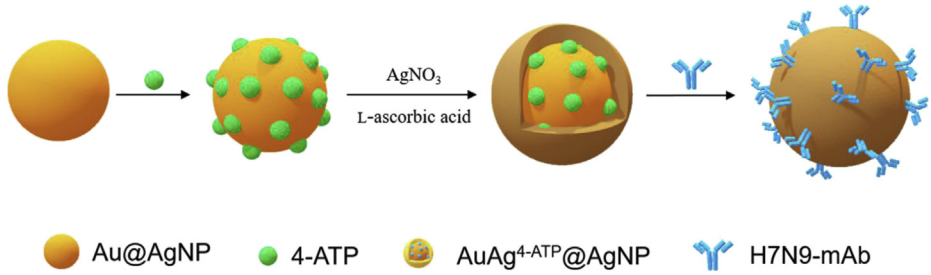

Fig. 1. Schematic representation of mAb-AuAg^{4-ATP}@AgNPs fabrication.

2.5. Detection of real AIV samples

Twenty H7N9 samples from different organs of poultry, including ten avian cloacal swab and ten throat swab samples, were collected and added to 1‰ formaldehyde to inactivate the virus at 4 °C overnight. After dilution, the samples, with antibiotics, were added to SERS-LFIAS. The Raman signal intensity was detected using a portable Raman spectrometer. For more in-depth analysis, a real-time PCR assay(more details in supplementary information) was used to assess the accuracy of the SERS-LFIAS tests.

3. Results and discussion

3.1. The mechanism of the SERS-LFIAS

The principle of the SERS-LFIAS is based on a sandwich-type immunoassay (Fig. 2a). In the presence of AIV H7N9, mAb-AuAg^{4-ATP}@AgNPs bind specifically to the AIV H7N9, forming immunocomplexes (antigen-mAb-AuAg^{4-ATP}@AgNPs). The immunocomplexes migrate along the NC membrane by capillary action. When the sample fluid reaches the test line, the immunocomplexes are captured by the capture antibody immobilized on the test line. Excess mAb-AuAg^{4-ATP}@AgNPs continue to migrate and are captured by the goat anti-mouse IgG antibodies immobilized on the control line (Fig. 2b). In the absence of avian influenza H7N9 virus, mAb-AuAg^{4-ATP}@AgNPs are only captured by the goat anti-mouse IgG antibody on the control line and just one line appears. The whole LFIA strip detection process is completed in 20 min.

To confirm whether or not the mAb-AuAg^{4-ATP}@AgNPs were captured on the test line, the SEM images for the corresponding of H7N9 virus were measured. In the absence of AIV H7N9, no immunocomplexes were formed in the test line (Fig. 3a). When the sample included 0.5 HAU AIV H7N9, the accumulation of immunocomplexes were observed in the paper fiber pores (Fig. 3b). Immunocomplex probes captured by the coated antibody on the test line can be, to some extent, observed by the naked eye. The Raman peak intensities of 4-ATP at 1580 cm^{-1} are determined from the average of the spectra collected at 10 different points in the middle of the test line and are recorded, for quantitative analysis.

3.2. Optimization of synthesis conditions for the Raman probe

AuAg^{4-ATP}@AgNPs was synthesized using a seeded growth strategy based on the stepwise reduction of $AgNO_3$ on the surface of AuNPs. We explored the effect of silver thickness on the AuAg^{4-ATP}@AgNPs Raman signal. The thickness of the silver layer on the surface of AuAg^{4-ATP}@AgNPs increased continuously along with gradual increase in the amount of $AgNO_3$. The solution color changed gradually from orange to brown (Fig. 4a). After increasing addition of $AgNO_3$, the UV/Vis absorption spectra revealed a red-shifted AuAg^{4-ATP}@AgNPs maximum absorption peak. When the concentration of $AgNO_3$ was 4.8 μM, the Raman signal of AuAg^{4-ATP}@AgNPs was the strongest and enhancement factor (EF) was determined to be 3.5×10^6 (Fig. S2), which is within the range that has been reported for 4-ATP on other substrates (10^4-10^6) [40,41]. However, with increasing addition of $AgNO_3$, the Raman signal began to decrease (Fig. 4b). Therefore, we settled on a 4.8 μmol amount of $AgNO_3$ to synthesize the AuAg^{4-ATP}@AgNPs.

3.3. Characterization of AuAg^{4-ATP}@AgNPs

The fabrication of the AuAg^{4-ATP}@AgNPs, containing Raman reporter molecules, which a thin silver layer was covered. There are several explanations for the improved SERS brightness of AuAg^{4-ATP}@AgNPs: (i) they possessed an intense electromagnetic field (E field) enhancement, (ii) the silver layer covering the Raman reporter molecules further enhanced the SERS, (iii) the presence of stable reporters protected inside the nanoparticles (iv) prevent the aggregation of Raman probe was prevented during testing. In this study, we synthesized an ultrabright SERS AuAg^{4-ATP}@AgNPs probe. The TEM characterization (Fig. 5a) indicated that the average size of the AuAg^{4-ATP}@AgNPs was approximately 36 nm, with a narrow size distribution and high monodispersity. The surface of AuAg^{4-ATP}@AgNPs was covered with a layer of silver. The EDS results showed that the nanoparticles were mainly composed of four elements, C, O, Ag, and Au, proving that the synthesis of AuAg^{4-ATP}@AgNPs was successful (Fig. 5b). The DLS results revealed that the average size of mAb-AuAg^{4-ATP}@AgNPs was somewhere in the range of 52 ± 6.5 nm (Fig. 6a). Compared to

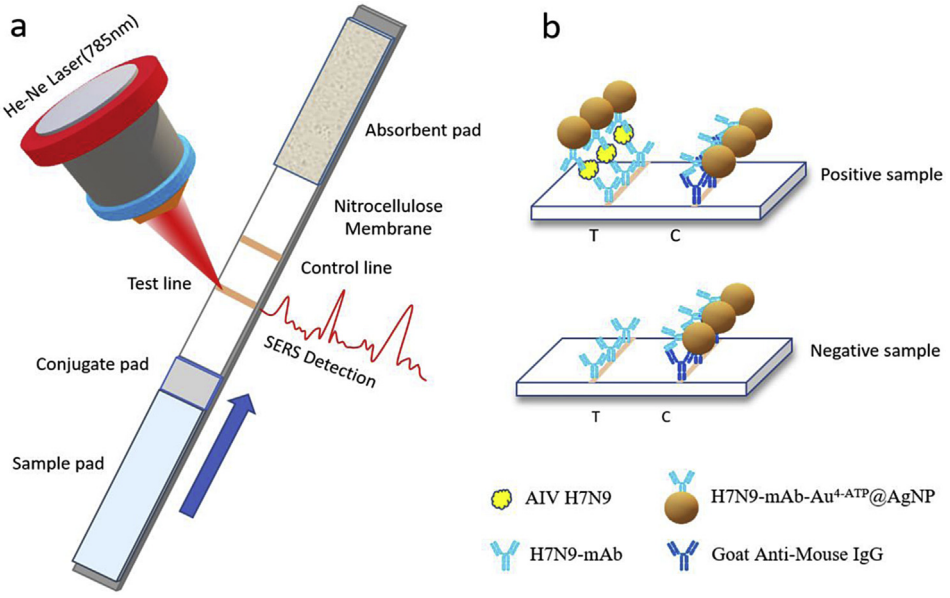

Fig. 2. (a) Schema of SERS-LFIAS-based detection of AIV H7N9. (b) For positive sample, two brown lines were observed on the test line and control line; For negative sample, and only one line appeared on the control line. (For interpretation of the references to color in this figure legend, the reader is referred to the Web version of this article.)

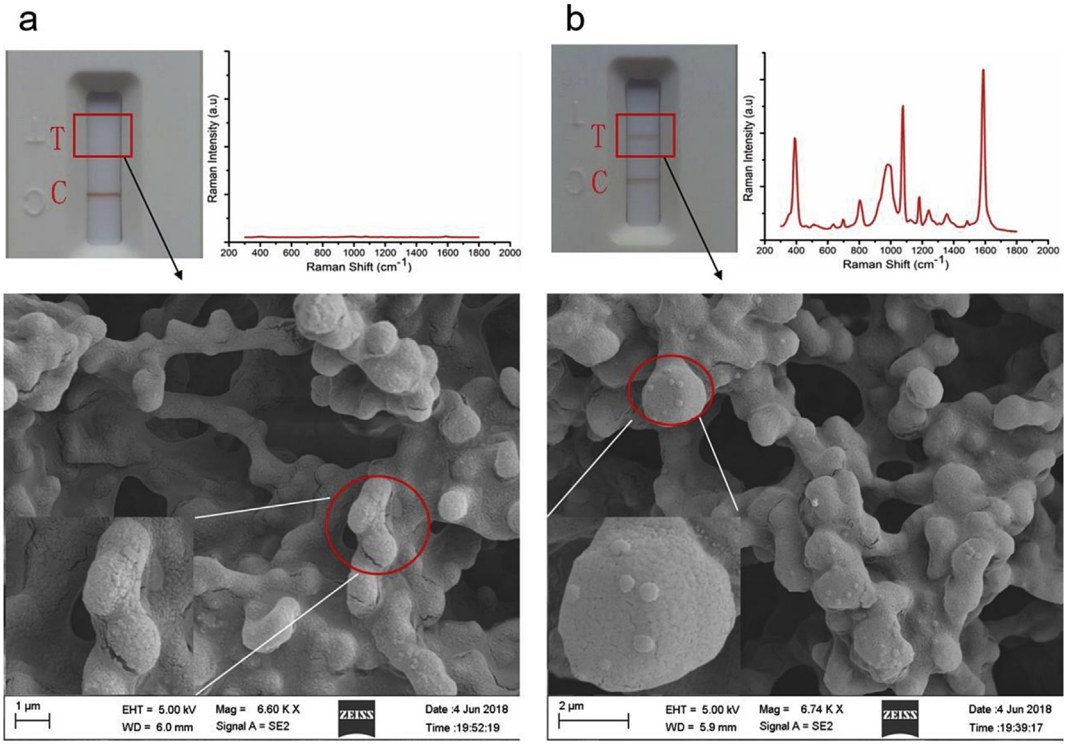

Fig. 3. Photographic image, SERS spectra, and SEM images of the SERS-LFIAS. (a) in the absence (off) of AIV H7N9 and (b) in the presence of AIV H7N9 (0.5 HAU).

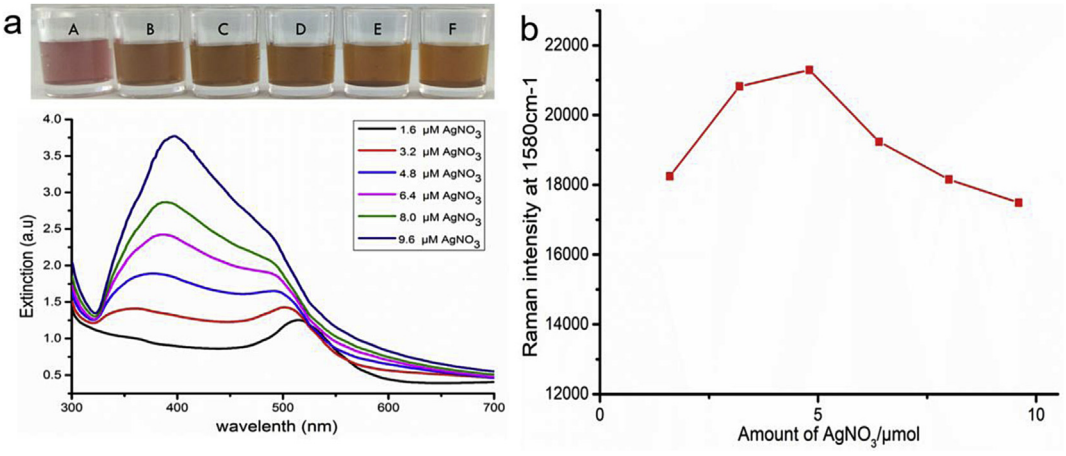

Fig. 4. Optimization of $AuAg^{4-ATP}$@AgNPs synthesis conditions. (a) The solution color and UV–Vis absorption spectra of $AuAg^{4-ATP}$@AgNPs with the amount of $AgNO_3$ added (A–F: 1.6 μM, 3.2 μM, 4.8 μM, 6.4 μM, 8.0 μM, and 9.6 μM silver nitrate, respectively.). (b) The Raman signal of $AuAg^{4-ATP}$@AgNPs with the amount of $AgNO_3$ added.

$AuAg^{4-ATP}$@AgNPs, the average size of mAb-$AuAg^{4-ATP}$@AgNPs increased by 16 nm, indicating that the antibody was successfully labeled on the surface of the nanoparticles. The average ζ-potential of $AuAg^{4-ATP}$@AgNPs for the encoded particles was −32.1 mV (Fig. 6b).

Furthermore, we evaluated the stability of mAb-$AuAg^{4-ATP}$@AgNPs and $AuAg^{4-ATP}$@AgNPs. The Raman intensities of $AuAg^{4-ATP}$@AgNPs were stable over a week. As time passed, the Raman signal began to decline slightly (Fig. S2). The color of the solution changed from the brown back to the original orange-yellow. We believed that the Raman reporter is exposed with oxidation of the silver layer. However, despite this concern, the $AuAg^{4-ATP}$@AgNPs showed excellent stability and were more stable for a long time after the antibody labeling.

3.4. Optimization of SERS-LFIAS

In order to improve the performance of SERS-LFIAS, we optimized several different parameters using 0.64 HAU AIV H7N9 as a positive sample and PBS as a negative sample. When the amount of anti-H7N9-mAb on the test line exceeded 0.5 μg/cm, and the Raman signal of the negative control was over 100 a. u. Here, we take 0.5 μg/cm anti-H7N9-mAb on the test as the optimum concentration. Furthermore, we investigated the amount of anti-H7N9-mAb labeled $AuAg^{4-ATP}$@AgNPs. When the amount of anti-H7N9-mAb labeled $AuAg^{4-ATP}$@AgNPs was 10 μg/mL, the SERS-LFIAS had the highest Raman signal (Fig. S4).

The stability of the antibody after labeling the nanoparticle is an important factor for the detection sensitivity. So, we tested 0.5 HAU

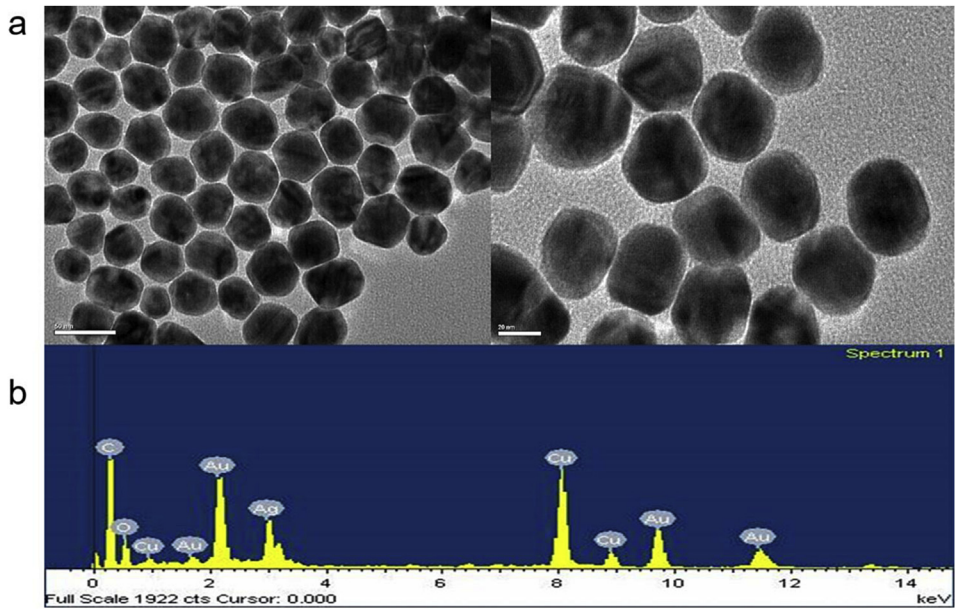

Fig. 5. Characterization of AuAg^{4-ATP}@AgNPs. (a) TEM images of synthesized AuAg^{4-ATP}@AgNPs at different magnifications (b) Composition of AuAg^{4-ATP}@AgNPs by EDS analysis.

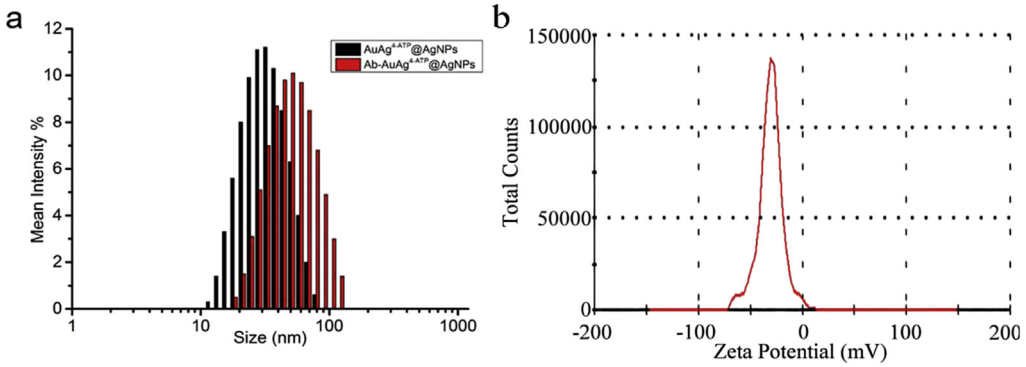

Fig. 6. (a) Dynamic light scattering data for the size distributions of AuAg^{4-ATP}@AgNPs (black column) and mAb-AuAg^{4-ATP}@AgNPs (red column). (b) The zeta potential of AuAg^{4-ATP}@AgNPs. (For interpretation of the references to color in this figure legend, the reader is referred to the Web version of this article.)

inactivated AIV H7N9 in the same batch of SERS-LFIAS every two days. As shown in Fig. S5, the T line Raman intensity of SERS-LFIAS (0.5 HAU inactivated AIV H7N9) decreased slightly for two weeks. It further confirmed the excellent stability of mAb-AuAg^{4-ATP}@AgNPs.

3.5. Quantitative analysis of AIV-H7N9 using SERS-LFIAS

Subsequently, we evaluated the sensitivity of SERS-LFIAS for AIV H7N9 detection under these optimal conditions. The SERS-LFIAS was used to detect virus titers ranging from 0.0025 to 2.56 HAU with three replicates. Briefly, samples of 2.56 HAU H7N9 virus were diluted two-fold with 0.015 M PBS (e.g. 2.56, 1.28, 0.64, 0.32, 0.16, 0.08, 0.04, 0.02, 0.01, 0.005 and 0.0025 HAU) and individually added onto the sample pad of a SERS-LFIAS. After 20 min, the Raman signals were read using a portable Raman spectrometer. As shown in Fig. 7A, the photographic images of SERS-LFIAS showed that the concentration of virus was directly related to the intensity of the color on the test line. Furthermore, images were analyzed using free image analysis software Image J and the results of gray values were used to construct standard curve (Fig. S6). The calculated LOD was estimated to be 0.068 HAU (LOD = yblank + 3 × SDblank). As we know, Raman is an ultrasensitive detection method that can detect invisible signals by the naked eye. In order to analyze this quantitatively, we needed to determine the sensitivity of our detection method and did so by measuring the Raman peak intensities on the T line. In order to obtain a reproducible intensity value, five different points from five independent experiments were averaged for the different concentrations of AIV H7N9. The results show that the intensity of the Raman peak increased along with increasing AIV H7N9 concentrations (Fig. 7B). The SERS peak intensities at 1580 cm $^{-1}$ were used to construct calibration curves (Fig. 7C). The LOD was estimated to be 0.0018 HAU, which was 3 orders of magnitude more sensitive than the hemagglutination assay (HA).

Furthermore, we assessed the precision and stability of SERS-LFIAS for the H7N9 virus detection. A series of H7N9 virus concentrations were assessed for the inter-assay and intra-assays. The intra-assays was test by same batches of SERS-LFIAS, which was store in a drying oven for 7 days, 14 days and 21 days at 37 °C. The Coefficient of Variance (CV) generated from triplicate experiments from both duplicate SERS-LFIAS batches and the same batch were high stability, indicating the stability of the SERS-LFIAS and their ability to be used in H7N9 virus detection (Table S2).

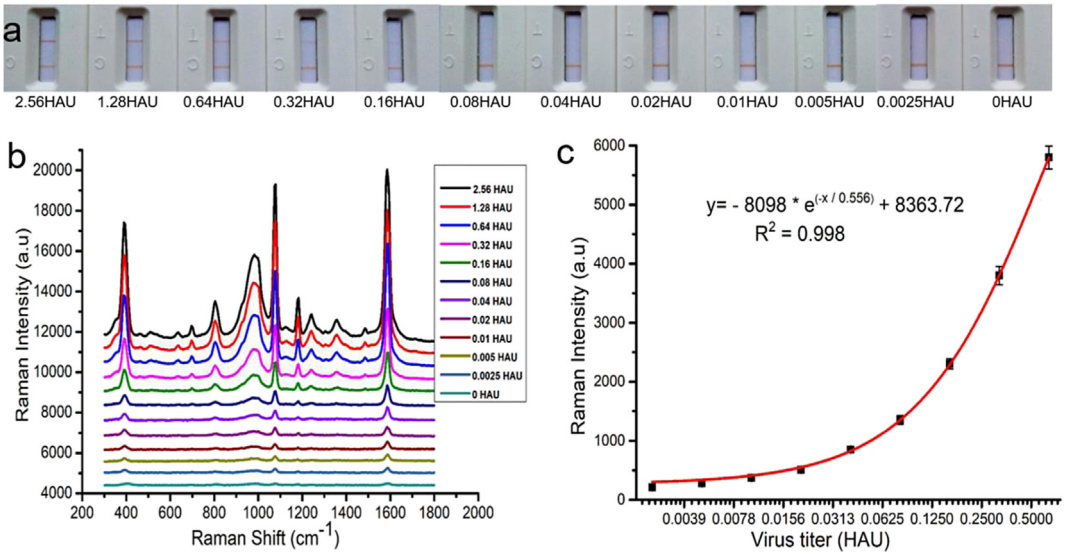

Fig. 7. Detection of AIV H7N9 with SERS-LFIAS. (a) Photographic image of SERS-LFIAS results for different concentrations of AIV H7N9. (b) Corresponding Raman spectra for the different concentrations of AIV H7N9. (c) The standard curve of the SERS-LFIAS IBS for AIV H7N9 detection ($R^2 = 0.998$).

Table 1
Method comparison for AIV detection.

Method	Detection target	Sensitivity (LOD)	Linear range	Time	Ref
QCM	H5N1 HA	0.0128 HAU	0.128–12.8 HAU	2 h	[42]
Impedance	H5N1 AIV	0.5 HAU	0.5–16 HAU	1 h	[43]
Amperometric	H5N1 AIV	0.00195 HAU	0.002–4 HAU	1 h	[44]
Fluorescence	H5N1 AIV	0.4 HAU	0.4–32 HAU	<30 min	[45]
SPR	H5N1 AIV	0.128 HAU	0.128–1.28 HAU	1.5 h	[46]
ECC	H5N1 AIV	0.0022 HAU	0.0025–0.16 HAU	1.5 h	[47]
Electrochemical	H7N9 virus gene	0.75 pM	1 pM-2.5 nM		[48]
IM-SPR	H7N9 AIV	144 (copies/mL)	2.3×10^2-2.3×10^5 (copies/mL)	<10min	[49]
Fluorescence	H7 subtype virus	40 HAU/mL	15–500 ng/mL	15 min	[50]
Enzyme-induced metallization	H7N9 AIV	1.25 pg/mL	5–150 pg/mL	30 min	[51]
Electrochemical	H7N9 AIV	7.8 fg/mL	0.01–1.5 pg/mL	2.5 h	[52]
Sandwich ELISA	H7N9 NA	6.25 ng/mL	–	–	[53]
SERS-LFIAS	H7N9 HA	0.0018 HAU	0.0025–0.5 HAU	20 min	this work

Notes: HA is AIV surface glycoprotein HA (Hemagglutinin); H7N9 viral gene refers to a fragment of the hemagglutinin gene sequence of AIV H7N9; H7 subtype virus refers to the AIV of the hemagglutinin subtype H7; NA is AIV surface glycoprotein NA (neuraminidase).

3.6. Comparison of analytical methods

A series of methods for the different subtypes of AIV detection have been reported in recent years. We compared the SERS-LFIAS developed in our study with the previous reported analytical methods for AIV detection, which is displayed in Table 1. Compared to most existing detection methods, the SERS-LFIAS method we established herein has a wider linear region and a lower detection limit comparatively. Although the high level of amplification that occurs in PCR-based testing yields a sensitive result, nucleic acid isolation requires trained operators, specialized instrumentation, and a higher value for time-cost. Additionally, the applications of electrochemical methods are complicated by complex electrode modification, unstable current, and environmental interference. As proposed in our SERS-LFIAS method, SERS tags could translate biomolecular recognition into a uniform Raman signal to form a color biosensor.

3.7. Specificity of the $AuAg^{4-ATP}$@AgNPs-LFIAS

To evaluate the selectivity of the SERS-LFIAS, we detected 0.32 HAU AIV H7N9 antigen as well as other subtypes of AIV and other

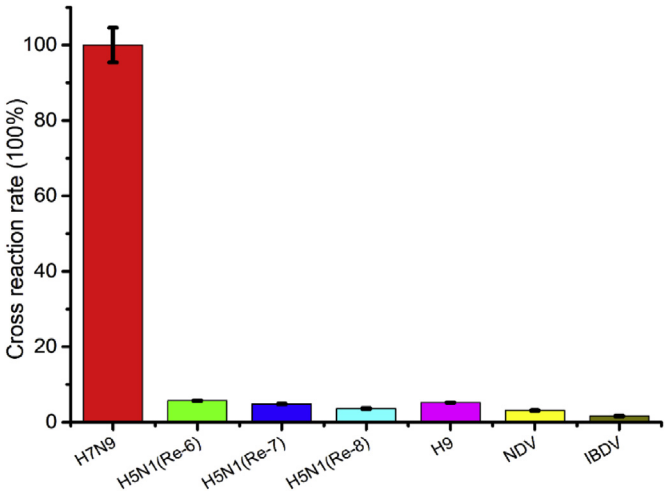

Fig. 8. The selectivity of SERS-LFIAS. The SERS peak intensities at 1580 cm^{-1} by AIV H7N9 and the other type avian virus (the concentrations of AIV H7N9 and other types of avian virus are 0.32 HAU).

Table 2
Reproducibility of SERS-LFIAS for AIV H7N9 detection.

Samples	Spiked concentration (HAU)	Detected by SERS-LFIAS (HAU)[a]	Raman intensity 1580 cm^{-1}	CV (100%)[b]
Avian cloacal swab	0.5	0.48 ± 0.047	3708.85	9.79
	0.1	0.094 ± 0.0083	1141.23	8.83
	0.02	0.018 ± 0.0013	398.34	7.44
	0.005	0.0042 ± 0.0003	247.65	7.62
	0	–	117.32	Out of linear
Throat swab	0.5	0.527 ± 0.0479	3926.08	9.1
	0.1	0.967 ± 0.0078	1165.35	8.07
	0.02	0.0184 ± 0.0012	402.54	6.74
	0.005	0.0052 ± 0.0037	263.36	7.12
	0	–	130.64	Out of linear

Notes:
[a] Results are expressed as the mean (n = 5).
[b] Coefficient of variation (CV) calculated as CV= (S.D./mean) × 100%.

Table 3
Sample tests using SERS-LFIAS and RT-PCR.

Samples	Number of samples	SERS-LFIAS result (P/N)	Real-time PCR result (P/N)
Avian cloacal swab	10	3/10	3/10
Throat swab	10	4/10	4/10

virulent infectious viral diseases found in chicken. The Raman signal of the T line is placed in the standard curve ($y = -8098*e^{(-x/0.556)}+8363.72$), the calculated virus titer that was equivalent to the Hemagglutination titer of AIV H7N9 (eH7N9) was obtained. The cross-reactivity rate is expressed as (eH7N9)/0.32 × 100%. The Raman signals from SERS-LFIAS for H7N9 subtypes virus reached high levels, whereas the Raman signals for other virus were close to blank values (Fig. 8). This result demonstrated that SERS-LFIAS were only responsive to very specific pathogens and possessed inherently high selectivity.

3.8. Sample tests

To investigate the feasibility of the SERS-LFIAS in real samples, a series of amounts of inactivated AIV H7N9 (e.g. 2.56, 1.28, 0.64, 0.32, 0.16, 0.08, 0.04, 0.02, 0.01, and 0.005 HAU) were added to avian cloaca swabs (Fig. S7). The calibration curves indicated that the LOD was 0.0035 HAU. Then, we used this calibration curves to analyze reproducibility of SERS-LFIAS in real samples. Avian cloacal swab and throat swab samples spiked with different concentrations of AIV H7N9 was tested. As shown in Table 2, the coefficient of variation (CV) are less than 10%, which demonstrates that the SERS-LFIAS is reproducible.

Next, twenty H7N9 samples from different organs of poultry were tested by SERS-LFIAS (Fig. S8) and the reference method of real-time PCR (Table S3). The results from SERS-LFIAS were basically consistent with real-time PCR results, indicating that SERS-LFIAS can rapidly detect H7N9 virus with a level of accuracy as high as comparable methods currently in use (Table 3). When compared to RT-PCR, SERS-LFIAS has the advantage of more simple operation because it does not require the trained operators, specialized instrumentation, sample purification, and the multiple steps that PCR-based methods demand. Thus, the SERS-LFIAS is promising as a potential method for rapid field detection.

4. Conclusions

In the current study, a novel SERS-based LFIAS was developed for rapid and highly sensitive detection of the AIV H7N9. The color change in the test line confirmed the presence of AIV H7N9, and quantification of the AIV H7N9 concentrations were obtained by averaging the SERS signals. Furthermore, the LOD of SERS-based LFIAS for the detection of AIV H7N9 was determined at 0.0018 HAU. Moreover, the proposed SERS-based LFIA strip sensor, exhibited a high level of sensitivity and capability for quantitative evaluation, giving it great potential of detecting the target antigen both quickly and sensitively in a simplified manner. In the future, changing the conjugation and capture antibody pairs, the SERS-LFIAS test could be easily extended to detect other types of pathogens. Overall, the SERS-LFIAS is a fast, simple, and ultra-sensitive immunoassay for the rapid detection of AIV subtypes H7N9, which could be used for on-site diagnostics.

Acknowledgments

This work was supported by the National Key Research and Development Program of China (2016YFD0500600).

Appendix A. Supplementary data

Supplementary data to this article can be found online at https://doi.org/10.1016/j.aca.2018.11.056.

References

[1] E.B. Bahadır, M.K. Sezgintürk, Trends Anal. Chem. 82 (2016) 286.
[2] R. Chapman, Y. Lin, M. Burnapp, A. Bentham, D. Hillier, A. Zabron, S. Khan, M. Tyreman, M.M. Stevens, ACS Nano 9 (2015) 2565.
[3] H. Jiao, Z.L. Zhang, C.Y. Wen, T. Man, L.L. Wu, L. Cui, Z. Lian, D.W. Pang, Anal. Chem. 88 (2016) 6577.
[4] C. Wang, F. Hou, Y. Ma, Biosens. Bioelectron. 68 (2015) 156.
[5] Y.K. Oh, H.A. Joung, H.S. Han, H.J. Suk, M.G. Kim, Biosens. Bioelectron. 61 (2014) 285.
[6] V.L. Schmit, R. Martoglio, K.T. Carron, A. Chem, Anal. Chem. 84 (2012) 4233.
[7] B. Kavosi, R. Hallaj, H. Teymourian, A. Salimi, Biosens. Bioelectron. 59 (2014) 389.
[8] X. Gao, H. Xu, M. Baloda, A.S. Gurung, L.P. Xu, T. Wang, X. Zhang, G. Liu, Biosens. Bioelectron. 54 (2014) 578.
[9] Y. He, X. Zhang, S. Zhang, M.K.L. Kris, F.C. Man, G. Liu, Biosens. Bioelectron. 34 (2012) 37.
[10] X. Liu, J.J. Xiang, Y. Tang, X.L. Zhang, Q.Q. Fu, J.H. Zou, Y. Lin, Anal. Chim. Acta 745 (2012) 99.
[11] J. Yan, Y. Liu, Y. Wang, X. Xu, Y. Lu, Y. Pan, F. Guo, D. Shi, Sensor. Actuator. B Chem. 197 (2014) 129.
[12] G.A. Posthumatrumpie, J.H. Wichers, M. Koets, L.B.J.M. Berendsen, A.V. Amerongen, Anal. Bioanal. Chem. 402 (2012) 593.
[13] Q.Y. Xie, Y.H. Wu, Q.R. Xiong, H.Y. Xu, Y.H. Xiong, K. Liu, Y. Jin, W.H. Lai, Biosens. Bioelectron. 54 (2014) 262.

[14] N.A. Taranova, A.N. Berlina, A.V. Zherdev, B.B. Dzantiev, Biosens. Bioelectron. 63 (2015) 255.
[15] K. Bobosha, E.M.T.K. Fat, S.J.F.V.D. Eeden, Y. Bekele, J.J.V.D.P. Schip, C.J.D. Dood, K. Dijkman, K.L.M.C. Franken, L. Wilson, A. Aseffa, PLoS Neglected Trop. Dis. 8 (2014) e2845.
[16] E. Juntunen, T. Myyryläinen, T. Salminen, T. Soukka, K. Pettersson, Anal. Biochem. 428 (2012) 31.
[17] Z. Li, Y. Wang, J. Wang, Z. Tang, J.G. Pounds, Y. Lin, Anal. Chem. 82 (2010) 7008.
[18] H.A. Joung, Y.K. Oh, M.G. Kim, Biosens. Bioelectron. 53 (2014) 330.
[19] S. Schlücker, Angew. Chem. Int. Ed. 53 (2014) 4756.
[20] J. Hwang, S. Lee, J. Choo, Nanoscale 8 (2016) 11418.
[21] X. Wang, N. Choi, Z. Cheng, J. Ko, L. Chen, J. Choo, Anal. Chem. 89 (2017) 1163.
[22] J.A.B. Ferreira, S.M.B. Costa, J. Phys. Chem. B 114 (2010) 10417.
[23] F.J.G.D. Abajo, Rev. Mod. Phys. 79 (2009) 1267.
[24] J. Song, B. Duan, C. Wang, J. Zhou, L. Pu, Z. Fang, P. Wang, T.T. Lim, H. Duan, J. Am. Chem. Soc. 136 (2014) 6838.
[25] X. Lu, M. Rycenga, S.E. Skrabalak, B. Wiley, Y. Xia, Annu. Rev. Phys. Chem. 60 (2008) 167.
[26] N. Gandra, C. Portz, S. Singamaneni, Adv. Mater. 26 (2014) 424.
[27] D.K. Lim, K.S. Jeon, J.H. Hwang, H. Kim, S. Kwon, Y.D. Suh, J.M. Nam, Nat. Nanotechnol. 6 (2011) 452.
[28] H.T. Ngo, N. Gandra, A.M. Fales, S.M. Taylor, T. Vo-Dinh, Biosens. Bioelectron. 81 (2016) 8.
[29] J. Li, Z. Zhi, B. Zhu, Y. Ma, B. Lin, R. Liu, Y. Song, L. Hui, T. Song, C. Yang, Anal. Chem. 88 (2016) 7828.
[30] N. Gandra, H.C. Hendargo, S.J. Norton, A.M. Fales, G.M. Palmer, T. Vo-Dinh, Nanoscale 8 (2016) 8486.
[31] Z. Yuan, W. Zhu, Y. Chen, P. Zhou, Z. Cao, J. Xie, C. Zhang, C. Ke, W. Qi, S. Su, Microb. Pathog. 64 (2013) 39.
[32] K.M. Pepin, J. Wang, C.T. Webb, G.J.D. Smith, M. Poss, P.J. Hudson, W. Hong, H. Zhu, S. Riley, G. Yi, Influenza & Other Respiratory Viruses 7 (2013) 97.
[33] J. Zhou, D. Wang, R. Gao, B. Zhao, J. Song, X. Qi, Y. Zhang, Y. Shi, L. Yang, W. Zhu, Nature 499 (2013) 500.
[34] D. Stamboulian, P.E. Bonvehí, F.M. Nacinovich, N. Cox, Infect. Dis. Clin. 14 (2000) 141.
[35] J.S. Ellis, M.C. Zambon, Rev. Med. Virol. 12 (2002) 375.
[36] M. Sánchezpurrà, M. Carrécamps, H.D. Puig, I. Bosch, L. Gehrke, K. Hamadschifferli, ACS Infect. Dis. 3 (2017).
[37] n.L. Blanco-Coviā, V. Montes-Garcā-A, A. Girard, M.T. FernÃ ndez-Abedul, J. Pā©Rez-Juste, I. Pastoriza-Santos, K. Faulds, D. Graham, M.C. Blanco-Lā³Pez, Nanoscale 9 (2017) 2051.
[38] M.L. Killian, Methods Mol. Biol. 436 (2008) 47.
[39] X. Ji, X. Song, J. Li, Y. Bai, W. Yang, X. Peng, J. Am. Chem. Soc. 129 (2007) 13939.
[40] J.A. Huang, Y.Q. Zhao, X.J. Zhang, L.F. He, T.L. Wong, Y.S. Chui, W.J. Zhang, S.T. Lee, Nano Lett. 13 (2013) 5039.
[41] K. Kim, H.B. Lee, J.Y. Choi, K.L. Kim, K.S. Shin, J. Phys. Chem. C 115 (2011) 13223.
[42] D. Li, J. Wang, R. Wang, Y. Li, D. Abi-Ghanem, L. Berghman, B. Hargis, H. Lu, Biosens. Bioelectron. 26 (2011) 4146.
[43] J. Lin, R. Wang, P. Jiao, Y. Li, Y. Li, M. Liao, Y. Yu, M. Wang, Biosens. Bioelectron. 67 (2015) 546.
[44] R. Wang, L. Xu, Y. Li, Biosens. Bioelectron. 67 (2015) 400.
[45] L. Xu, R. Wang, L.C. Kelso, Y. Ying, Y. Li, Sensor. Actuator. B Chem. 234 (2016) 98.
[46] H. Bai, R. Wang, B. Hargis, H. Lu, Y. Li, Sensors 12 (2012) 12506.
[47] Q. Zhang, L. Li, Z. Qiao, C. Lei, Y. Fu, Q. Xie, S. Yao, Y. Li, Y. Ying, Anal. Chem. 89 (2017).
[48] S. Dong, R. Zhao, J. Zhu, X. Lu, Y. Li, S. Qiu, L. Jia, X. Jiao, S. Song, C. Fan, ACS Appl. Mater. Interfaces 7 (2015) 8834.
[49] Y.F. Chang, W.H. Wang, Y.W. Hong, R.Y. Yuan, K.H. Chen, Y.W. Huang, P.L. Lu, Y.H. Chen, Y.A. Chen, L.C. Su, Anal. Chem. 90 (2018).
[50] S.J. Yeo, D.T. Bao, G.E. Seo, C.T. Bui, D.T.H. Kim, N.T.V. Anh, T.T.T. Tien, N.T.P. Linh, H.J. Sohn, C.K. Chong, Sci. Rep. 7 (2017) 7933.
[51] H. Zhang, X. Ma, S. Hu, Y. Lin, L. Guo, B. Qiu, Z. Lin, G. Chen, Biosens. Bioelectron. 79 (2016) 874.
[52] Z. Wu, W.J. Guo, Y.Y. Bai, L. Zhang, J. Hu, D.W. Pang, Z.L. Zhang, Anal. Chem. 90 (2017).
[53] Y. Yu, Z. Xi, B. Zhao, S. Ying, X. Zhang, B. Tian, L. Jian, L. Zi, L. Liu, D. Wang, J. Virol Methods 247 (2017) 58.